ZDES of jets aeroacoustics: recent progress with unstructured grids and challenges

Fabien Gand, Maxime Huet, Thomas Renaud, Fulvio Sartor

ZDES of jets aeroacoustics: recent progress with unstructured grids and challenges

Fabien Gand[1], Maxime Huet[2], Thomas Renaud[1], Fulvio Sartor[1]
[1]DAAA, ONERA, Université Paris Saclay, F-92190 Meudon, France
[2]DAAA, ONERA, Université Paris Saclay, F-92322 Chatillon, France

This paper presents scale resolving simulations for jet noise prediction of configurations of increasing complexity. In order to deal with geometrically complex configurations, the unstructured mesh approach is considered in this work, which is a departure from previous studies by the Authors. Therefore, the simulation methodology based on Zonal Detached Eddy Simulation mode 3 (Wall Modelled LES) and unstructured grids is first validated on an isolated M_j=0.9 jet and compared to previous results with structured grids, which emphasizes the major improvements achieved. This approach is then used to investigate jet/surface interaction (JSI) noise on an academic configuration. The simulations results are scrutinized in order to evidence the diffraction of the wavepackets associated with the jet by the trailing edge of the surface, and how the jet exit Mach number and jet/plate distance influence this phenomenon. Finally, the methods validated in the first two sections are applied to a business-jet-type configuration composed of a dual mixed flow nozzle, a fuselage and a horizontal tail plane. Each of these three complementary studies brings into focus some challenges related to the numerical methods used for the prediction of jet noise. Of interest, this work is supported by the European Project DJINN.

I. Nomenclature

D	=	Nozzle exit diameter
δ	=	Boundary layer thickness
L	=	Streamwise distance from the nozzle exit to the plate trailing edge
h	=	Vertical distance between the jet axis and the plate
St	=	Strouhal number based on the nozzle exit diameter
M_j	=	Jet exit Mach number

II. Introduction

Along with greenhouse gas emissions, the reduction of aircraft noise is a major concern for sustainable aviation. In this regard, European Union's FlightPath 2050 [1] set ambitious targets toward the reduction of the environmental footprint of aviation which include a 65% reduction of perceived aircraft noise relative to typical new aircraft in 2000. The reduction of engine jet noise and its interaction with the airframe is a key issue regarding the achievement of this goal since it is the major source of aircraft noise at take-off and during climb, which are flight stages strongly affecting surrounding populated areas.

In this framework, the design of low-noise aircraft requires accurate and reliable simulation tools to predict jet noise and installation effects as well as a detailed understanding of the physics involved in jet noise generation. However, despite significant progress in numerical methods, modelling and computing power achieved over the last decades,

[1] Research scientist, Aerodynamics, Aeroelasticity, Acoustics Department, F-92190 Meudon, France
[2] Research scientist, Aerodynamics, Aeroelasticity, Acoustics Department, F-92322 Chatillon, France

the simulation of jet noise remains a challenging topic for CFD [2] [3] [4]. Indeed, jet noise numerical predictions require both the computation of the noise sources – i.e. turbulence – and efficient propagation of acoustic waves towards the observation point. The underlying challenges of both of these issues are numerous, and can be conflicting.

This paper, carried out in the framework of the European Project DJINN [5], presents a set of three complementary studies aimed at improving the simulation methodology used to predict jet noise for technical configurations. The main increment compared to previous studies by the Authors is the use of unstructured meshes. As a matter of fact, a number of studies (including previous work by the Authors) have stressed out the difficulties and limitations associated with the use of structured grids for complex geometries [6] [7] [8] [9] [10]. On the other hand, significant improvements have been achieved over the last decade in the generation and management of unstructured meshes as well as in the efficiency of the CFD solvers for such meshes [11] [12] [4] [13] [14] [15] [16] [17] [18].

The paper is organized as follows. First, the computational methods used for the CFD solver, the turbulence modelling, and the noise radiation process are presented. The numerical approach is then assessed on a well-documented isolated jet case [19]. Of interest, simulations with structured and unstructured meshes are compared in order to lay emphasis on the benefits and shortcomings of each approach. In the fourth section of the paper, the simulation process based on unstructured meshes is put to use for the investigation of jet/surface interaction (JSI) noise. A special focus is made to ensure that the simulations reproduce the main features of the JSI noise generation mechanisms. Finally, the methods validated in the first two sections are applied to a business-jet-type configuration composed of a dual mixed flow nozzle, a fuselage and a horizontal tail plane.

III. Computational methods

A. CFD solver settings

All CFD simulations presented in this paper were performed with the elsA software (ONERA-Safran property) [20]. The time integration scheme is common to structured and unstructured grid simulations and relies on a 2^{nd} order accurate implicit backward differencing scheme with a timestep of 1 µs (corresponding to a maximum CFL number based on the maximum acoustic velocity of 15 in the shear layer) and a number of inner sub-iterations adapted in each simulation to ensure a decrease of at least 1 order of magnitude of the residuals during the sub-iteration process. For both types of grids, the diffusive fluxes are discretized using a second-order-accurate centered scheme.

In the case of structured grids, the convective terms are treated with a hybrid centered/upwind second-order-accurate modified AUSM+P scheme [21] using a MUSCL extrapolation of the third order. This version of the AUSM+P scheme involves a "wiggle" sensor to minimize numerical dissipation by applying some upwinding only in areas where the solution displays numerical oscillations, while the scheme is actually centered everywhere else [21]. For unstructured grids, the choice of the numerical settings was guided by best practices based on previous works and features available for such meshes in the software. The spatial discretization is 2^{nd} order accurate and relies on a 1-exact flux reconstruction at cell interfaces. The convective fluxes are computed with a Roe scheme. The gradients are computed with a Green-Gauss approach. It is noteworthy that the CPU cost of the present simulations is very similar for the structured and unstructured cases.

B. Turbulence modelling: Zonal Detached Eddy Simulation and turbulence generation

The hybrid RANS/LES approach used in this work is the Zonal Detached Eddy Simulation (ZDES) [22] developed at ONERA. This approach has been used with success to simulate a wide range of applications of industrial interest [23]. One of the advantages of the ZDES is its flexibility; indeed, ZDES covers several types of turbulent flows, which can be combined. In particular, mode 3 is devoted to WMLES, which is the resolution level required for the nozzle boundary layer for jet noise studies [19] [24] [25] . An example of the combined use of the three modes of ZDES within the same computation can be found in Ref [26].

The ZDES is based on the basic idea of the original Detached Eddy Simulation [27] (DES97) which relies on a length scale substitution on the destruction term of the Spalart-Allmaras (SA) RANS model [28]. Depending on the ZDES mode selected, a hybrid length scale and a specific subgrid length scale are defined. Of interest, ZDES mode 2 (2020) [29] makes use of a shielding function f_p to detect automatically attached boundary layers to be treated in RANS mode without any user intervention which will be used to compute the parts of the airframe where no noise sources are generated but where the prediction of attached boundary layers is important. The reader is referred to reference publications [22] [30] [29] for a detailed description ZDES formulation.

The initial conditions of jet flow development are critical for the accuracy of the simulations for jet noise prediction [2] [25] [19] [24] [11] [4]. As a matter of fact, in case of turbulent jets, the nozzle boundary layer needs to be resolved and the laminar/turbulent transition in the nozzle boundary layer must be triggered. To this effect, a methodology based on the use of roughness elements – or tripping cylinders – was proposed by Deck et al. [31] and applied successfully to jet flow simulations in [24]. It is reminded that the principle of this approach is to introduce streamwise vorticity inside a boundary layer which has no resolved fluctuations at the height where it is most likely to be amplified, and therefore trigger transition. Thanks to this physics-based approach, almost no spurious noise is produced by the turbulence generation devices, which is a key feature for aeroacoustics simulations. Besides, the use of Immersed Boundary Conditions to introduce the roughness elements in the computational domain makes this method rather easy to implement and setup.

C. Noise radiation

Far field pressure time signals are reconstructed from the unsteady aerodynamic flow fields extracted on surfaces surrounding the jet in the near field, using the Ffowcs Williams and Hawkings (FWH) integral formulation [32] implemented in the ONERA KIM software. As illustrated in Fig. 2, three surfaces with different radial extensions are used to ensure the stability of the noise radiation process (*i.e.* to check the independence of the results on the location of the surface). Those surfaces are closed at both extremities using the additional flux terms proposed by Rahier et al. [33]. This methodology differs from the ones traditionally used in jet noise radiation problems, where the surfaces are kept open [11] [12] [8] or where an averaging of the flow quantities is achieved on several downstream discs [19] [34] [35] to avoid spurious noise radiation caused by the turbulence crossing the storage surface. With the additional flux terms, spurious radiation from turbulence becomes negligible compared to the physically radiated noise. The advantages of this new formulation are manifold [33]. In particular, it improves the stability of the noise computed from the different surfaces, especially in the low frequency part of the spectra.

For installed jets presented in section V, two noise radiation procedures are considered. In the first approach, the porous surface encloses the jet plume and the solid surface to account for all the noise sources and interactions with the plate in the CFD simulation. In the second approach, the noise radiation methodology for free jets is adapted to the presence of the plate in order to limit the computational cost of the post-processing. This is achieved by limiting the storage of the unsteady flow fields to the region of the noise sources, so that the storage surfaces do not enclose the entire plate along the spanwise direction. Instead, a two-step radiation methodology is used. The porous surfaces used for noise radiation are limited to the jet plume and jet/plate interaction area, as illustrated in Fig. 1 (b). In a first step, the noise sources included inside the surface, namely the jet and jet-plate interaction noise sources, are radiated to the observers. The acoustic reflections on the plate outside the storage surface are modelled in a second step. The final acoustic signals are obtained by summing up both contributions. This innovative approach is thoroughly presented and assessed in [36] and [37]. The two approaches provide identical results and are used indifferently in the section.

In the following, the power spectral densities and integrated levels follow the $1/M_j^4$ scaling proposed by Brès et al. (see Eq. B 8 of [19]).

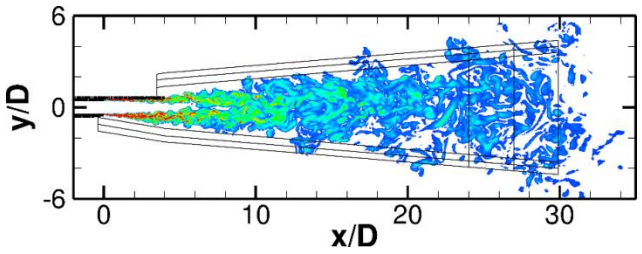

(a) Detailed position of the storage surfaces

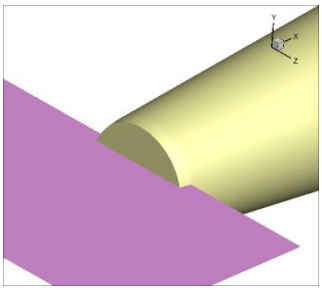

(b) Illustration of the noise modelling procedure. Porous surface is in yellow, flat plate (reflective surface) is in purple

Fig. 1. Location of the storage surfaces for the FWH solver for installed jets simulations

IV. Unstructured mesh approach validation on an isolated jet

In this section, the focus is put on the assessment of the accuracy of the unstructured mesh simulations and the comparison with structured grid simulations. A complete analysis of the results, including a statistical convergence study, can be found in [37]. The results presented in this part correspond to a simulation time of 300 D/U which was found to be sufficient for isolated jet since azimuthal averaging can be carried out [37].

A. Description of the test case and meshes

The jet studied in this section is an isolated single stream jet investigated experimentally in the Pprime laboratory (based in Poitiers, France) [19]. The exhaust Mach number is equal to M_j=0.9, the nozzle exit diameter is D=0.05 m, the nozzle pressure ratio is Pi/P_0=1.7 and the nozzle temperature ratio is Ti/T_∞=1.15. The Reynolds number based on the diameter is equal to $Re_D=10^6$ and the boundary layer inside the nozzle is tripped, so that the flow is fully turbulent at the nozzle exit. Noise levels are captured on a polar antenna located 50 diameters from the nozzle exit. All experimental data and nozzle geometry are available online [19]. The geometry of the convergent-straight nozzle and the computational domain used for all simulations are shown in Fig. 2.

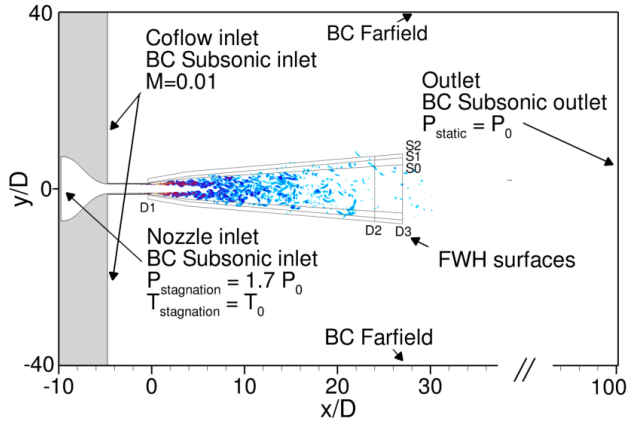

Fig. 2. Computational domain

Mesh name	Mesh count ($/10^6$)				
	Nozzle inlet	BL	Shear layer	Plume + farfield	Total
Structured-Grid1BL	-	-	-	-	54
Structured-Grid2BL	-	-	-	-	156
Unstructured-Mesh1	5	10	19	40	74
Unstructured-Mesh2	5	10	41	88	144
Unstructured-Mesh3	11	10	41	120	182

Table 1. Grid sizes

As mentioned in the Introduction, the main objective of the present section is to assess the use of ZDES with unstructured grids. To this effect, three unstructured meshes of increasing density have been generated (see grid counts in Table 1), and the coarsest mesh level is illustrated in Fig. 3. In order to quantify the improvements achieved with this approach, the results are compared to previous simulations carried out with structured grids [24]. Both grid types are depicted in Fig. 3 where one can observe the salient differences between the meshing techniques, in particular the ability to cluster grid points very locally with the unstructured approach without propagating grid refinements throughout the computational domain. The use of isotropic cells in the early stages of the shear layer and in the jet mixing area in the unstructured mesh is also considered beneficial for LES.

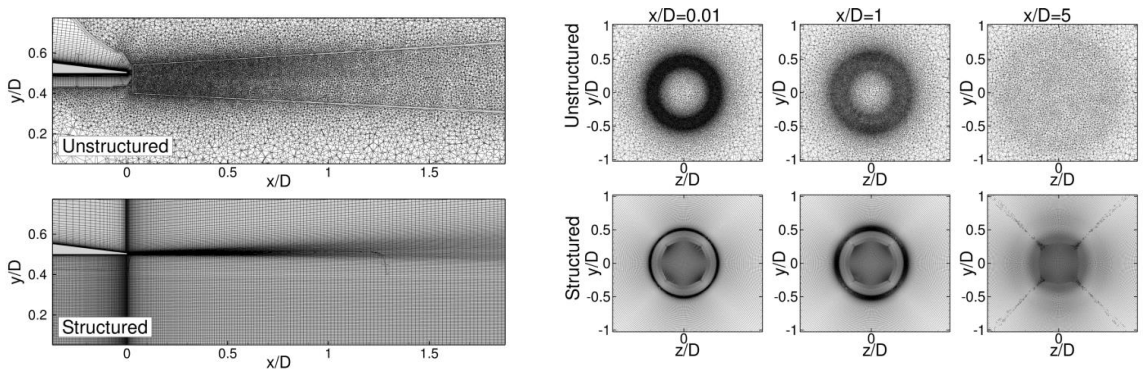

Fig. 3. Visualizations of structured (Grid2BL) and unstructured (Mesh1) meshes

The plots in Fig. 4 provide some quantitative comparisons of the meshes cell sizes. In structured grids, total grid count limitations lead to restrictions in streamwise and azimuthal grid resolutions and in turn to highly anisotropic cells in the jet plume. On the other hand, isotropic cells are used in the jet plume with unstructured meshes, and the resolution follows the physical constraints of the jet flow development: small cells (in all directions, contrary to what was achievable with structured grids) are used near the nozzle exit and the cell size is progressively enlarged as the coherent structures grow in the jet shear layer.

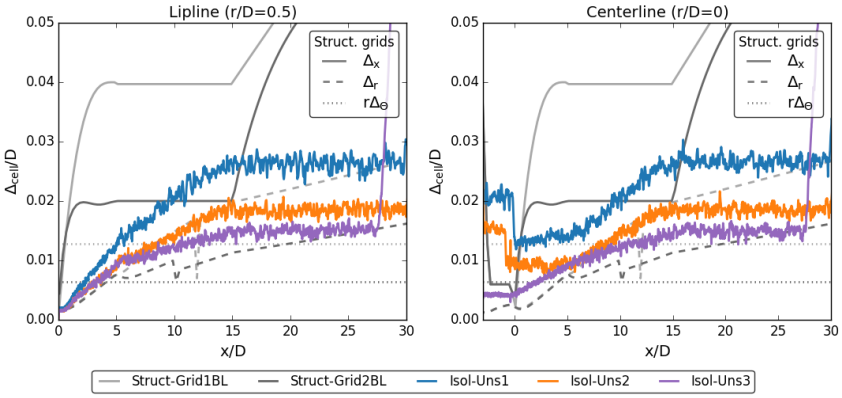

Fig. 4. Mesh sizes for the isolated jet simulations

B. Results

Instantaneous visualizations of the simulations are shown in Fig. 5 for each grid. The development of a turbulent boundary layer inside the nozzle thanks to the turbulence generation method mentioned in section IIIB [31] appears similar in all cases, even though smaller eddies seem to be captured with the structured grid. This is attributed to the low dissipation spatial scheme used, which was not available for unstructured grids when the simulations were performed. The low dissipation scheme also provides a better propagation of the acoustic waves – at least visually, this aspect is quantified in the next sections. From these visualizations, the increase of the unstructured grid density does not seem to bring any significant improvement, even if smaller eddies appear to be better resolved in the aft part of the jet with Mesh3.

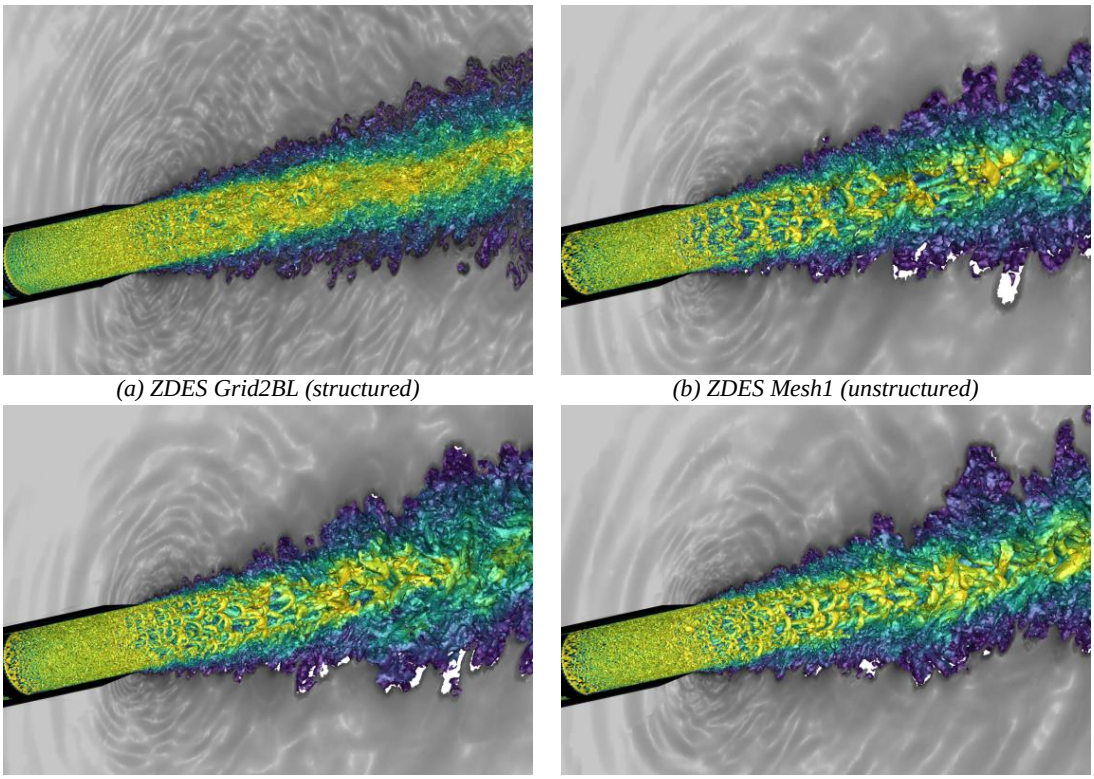

(a) ZDES Grid2BL (structured) *(b) ZDES Mesh1 (unstructured)*

(c) ZDES Mesh2 (unstructured) *(d) ZDES Mesh3 (unstructured)*

Fig. 5. Iso-surfaces of Q criterion (color) and density gradient magnitude (grayscale)

In order to verify that the initial conditions of the jet are the same for all cases, nozzle exit boundary layer profiles are plotted in Fig. 6. All simulations are in fair agreement with the experimental data and reference simulation data from [19]. This verification is mandatory to ensure that the results and their analysis are not biased by differences in the jets initial conditions.

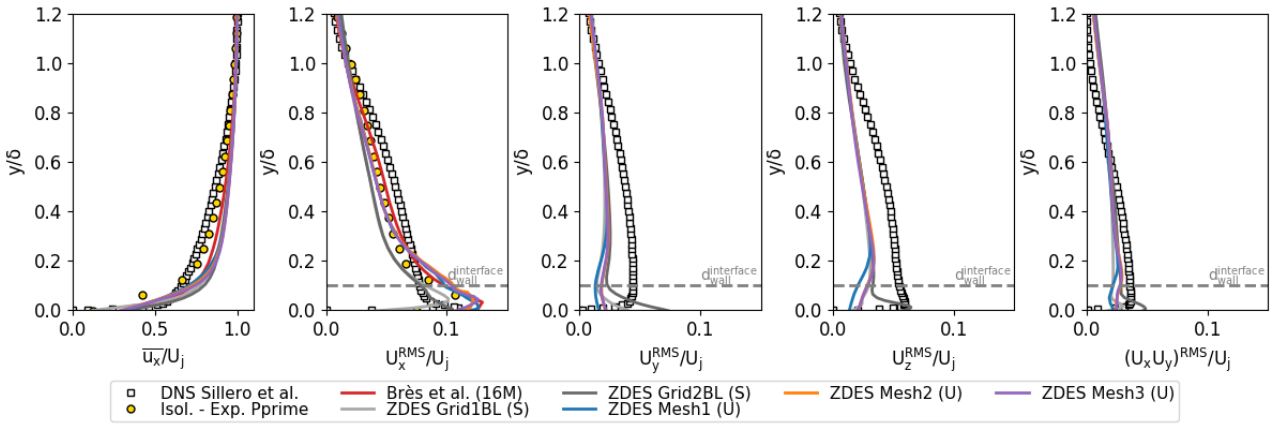

Fig. 6. Nozzle exit boundary layer profiles. The horizontal dashed line on the right hand side plots represents the location of the RANS/LES interface used for the ZDES mode 3 modelling. (S): structured grids, (U): unstructured grids

The jet flow and shear layer development can be analyzed with the curves in Fig. 7. These plots provide a quantified assessment of the improvement achieved with the unstructured simulations. The jet potential core length is correctly captured as well as the level and location of the peak of streamwise velocity fluctuations with all unstructured mesh simulations, which was not the case with the structured grid simulations. Furthermore, the results are almost

unchanged with the increase in unstructured grid density whereas the detrimental effect of the structured grid refinement was acknowledged in [24] and attributed, at least partly, to the anisotropy of the cells.

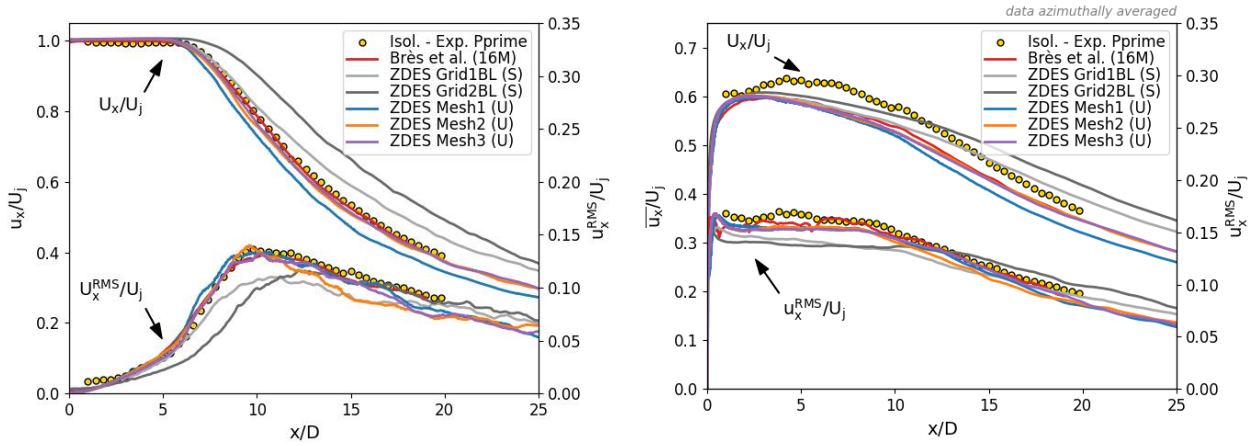

Fig. 7. Mean and RMS velocity profiles along the jet centerline (left) and lipline (right). (S): structured grids, (U): unstructured grids

In terms of spectral content, the benefits of the structured grid approach – along with a low-dissipation scheme – are evidenced by the plots in Fig. 8. Indeed, the frequency cutoff is generally larger for the simulations with structured grids in these figures, particularly in the fully developed part of the shear layer and jet mixing area (Fig. 8 (b) and (d)). On the other hand, close to the jet exit (Fig. 8 (a) and (c)), one can see that the clustering of mesh cells in the simulations with unstructured meshes seems to compensate the larger dissipation of the numerical scheme. The frequency cutoff of the spectra from these simulations is also slightly increased with the mesh refinement.

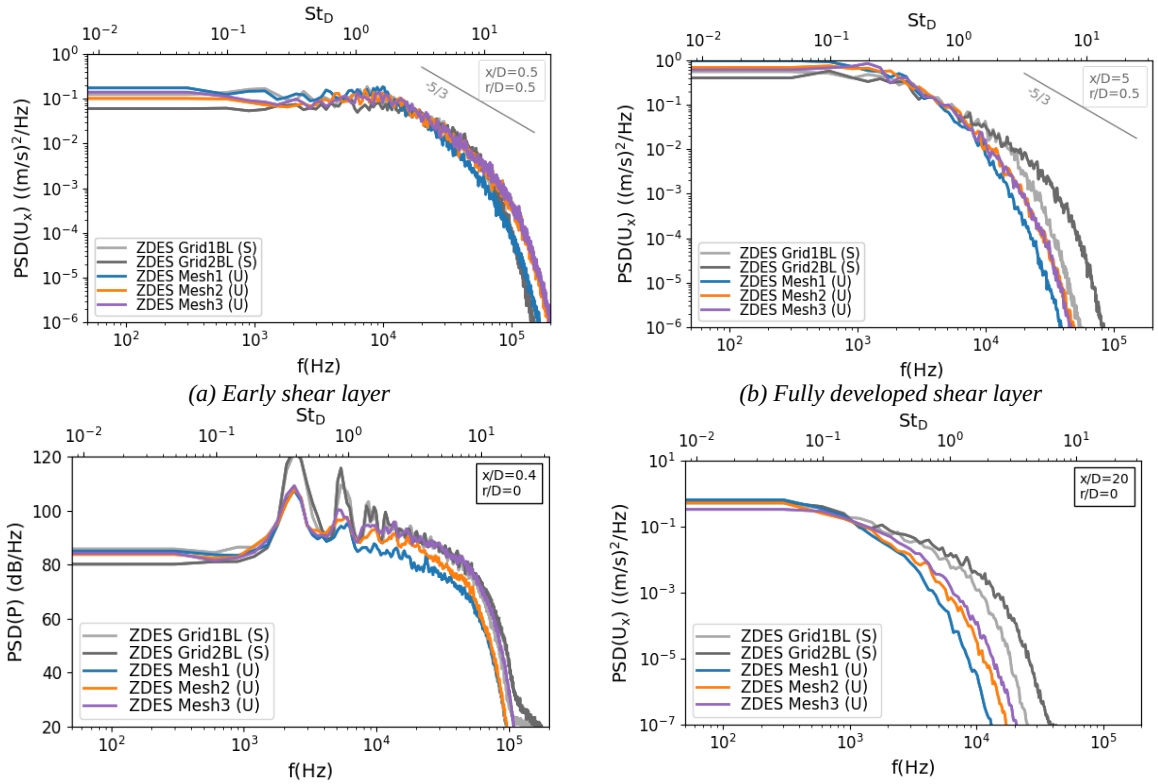

(a) Early shear layer

(b) Fully developed shear layer

(c) Jet centerline, close to nozzle exit

(d) Jet centerline, mixing area

Fig. 8. Selected streamwise velocity and pressure spectra. (S): structured grids, (U): unstructured grids

Finally, the increased accuracy obtained with the simulations with unstructured grids for jet noise prediction is highlighted in Fig. 9 and Fig. 11. The structured grid simulations systematically under predict the low frequency levels of the spectra and their peak, which is consistent with the analysis of the aerodynamic fields presented above and leads to a disappointing under prediction of 1 to 3 dB of the integrated pressure levels (Fig. 11).

Conversely, the unstructured grid simulations provide a fairly good agreement with the experiments for a wide range of frequencies in Fig. 9. The farfield noise results are detailed in [37] and show that with an extraction surface located in the jet vicinity (S0 in Fig. 2 and in the top picture of Fig. 9), the noise spectra visible in Fig. 10 are accurately predicted up to St=8 (which is the largest frequency resolved in the experimental dataset), with however a small underprediction of the levels for St > 2 with Mesh1. The integrated far-field noise levels are captured within less than 1dB for all observer angles (Fig. 11), which is comparable with state-of-the-art numerical results published [19].

These results, along with all flow data presented in this section, provide a fair assessment of the ZDES simulations with unstructured grids and validate the use of this approach for further investigations on more complex geometries. First steps in this direction are provided in sections V and VI.

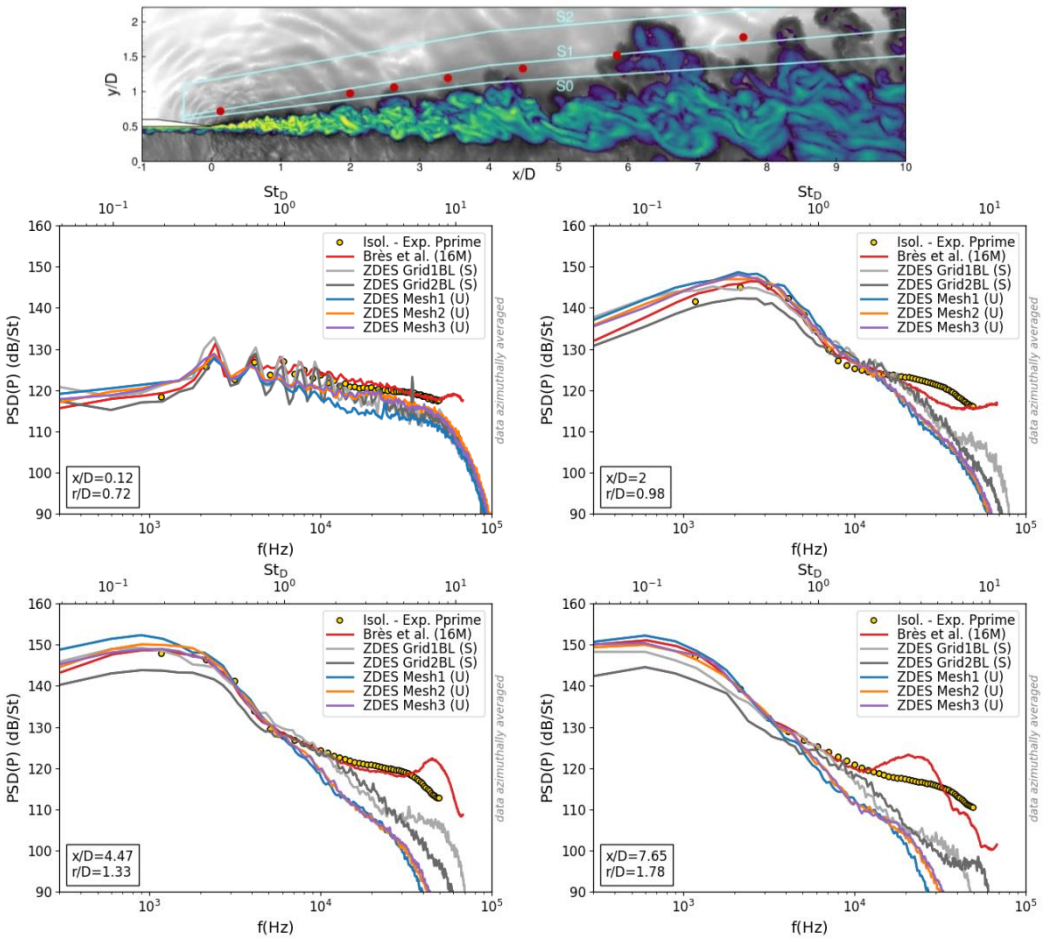

Fig. 9. Near field pressure spectra extracted for the CFD simulations (selected probes among the red dots in the top picture). (S): structured grids, (U): unstructured grids

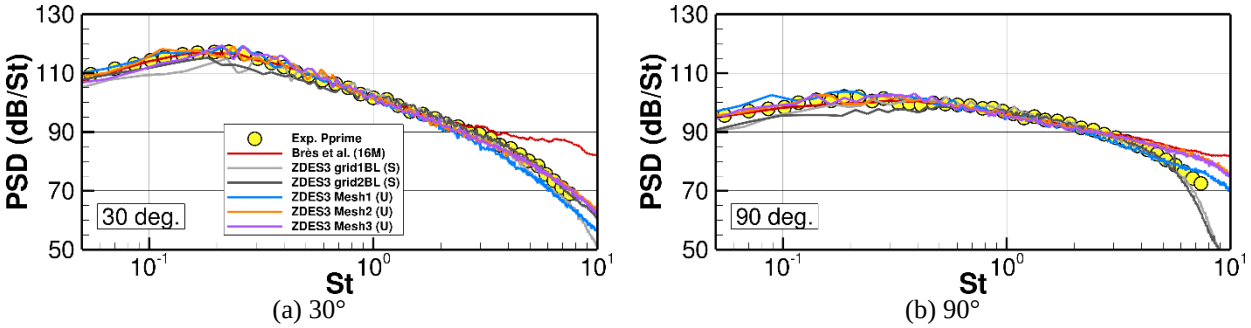

(a) 30° (b) 90°

Fig. 10. Power-spectral densities of the far-field radiated noise on the polar antenna, located 50D from the nozzle exit.

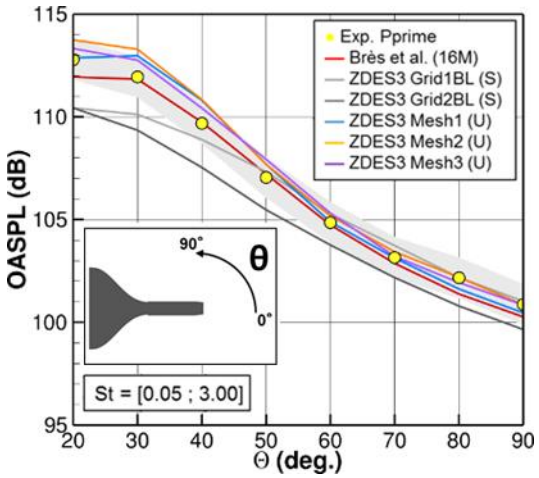

Fig. 11. Integrated pressure levels in the jet far-field after far-field noise radiation. The polar antenna is located 50D from the nozzle exit. (S): structured grids, (U): unstructured grids. The gray zone corresponds to the experiments +/- 1dB.

V. Jet surface interaction investigation

The unstructured mesh approach validated in the previous section is used to investigate some aspects of jet/surface interaction in this section. A complete description of the methods used for noise radiation can be found in [37]. As an introduction to this section, it is reminded that the main physics underlying the jet/surface interaction noise is the diffraction of isolated jet noise sources (turbulent wavepackets) by the trailing edge of the surface [38] [39] [40]. Furthermore, it has been shown that this phenomenon is well accounted for by linear models [41] [42] [43]. The linearity of the JSI noise is actually a key property used to derive active noise reduction techniques [42] [43] [44].

A. Description of the test case and meshes

In order to investigate jet surface interaction, a flat plate is placed above the jet studied in the previous section. As illustrated in Fig. 12, two positions of the plate are considered in this paper. This setup was extensively used in wind tunnel tests at the Pprime Laboratory in Poitiers, France [40] [44]. The baseline jet flow conditions (M_j=0.9) are the same as the ones given in section IV.A. The external flow is at rest. Noise characterization is performed on an azimuthal antenna of radius 14.3D, composed of 18 evenly distributed microphones.

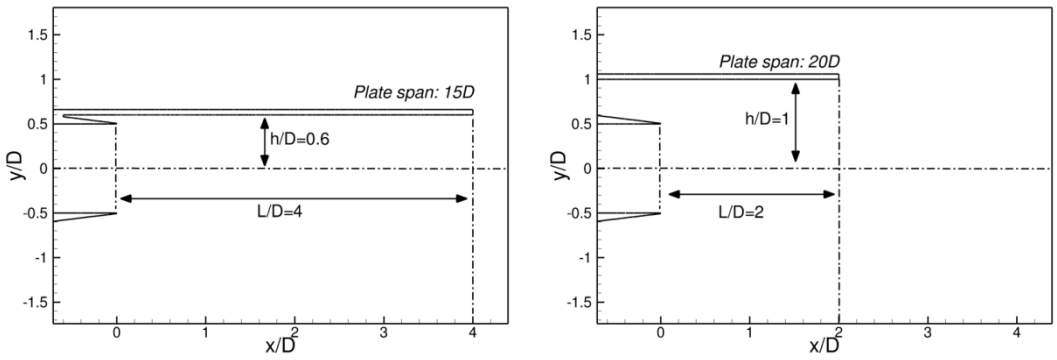

Fig. 12. Jet/plate configurations investigated

The numerical setup used in section IV is reproduced for the installed jet simulations. As depicted in Fig. 13, the unstructured meshing approach makes the generation of the mesh straightforward. The mesh density of Mesh1 of the isolated jet (see Table 1 and Fig. 4) was used here since it was shown to provide a very good agreement with experiments and only minor improvements were brought on with Mesh2 and Mesh3.

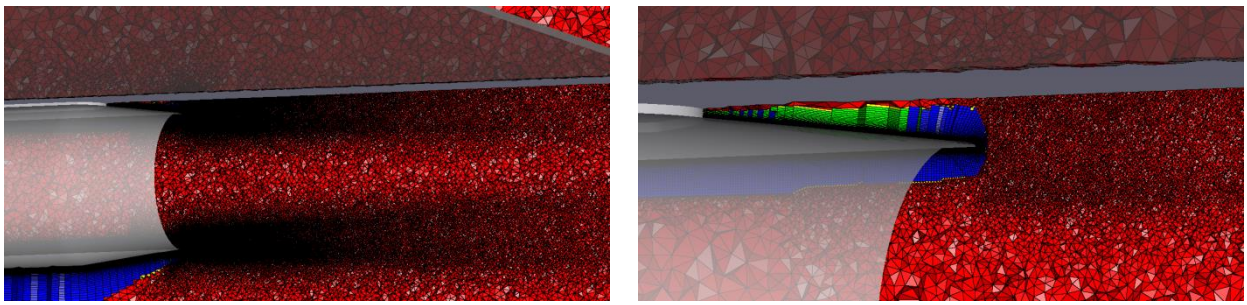

Fig. 13. Illustration of the mesh used for the installed jet h/D=0.6, L/D=4. Green: prisms, blue: hexahedra, yellow: pyramids, red: tetrahedra

B. Effect of the position of the plate

The diffraction by the plate trailing edge of the wavepackets developing in the shear layer of the jet is supposed to be the main contributor to the jet/surface interaction [40] [44]. Therefore, the amplitude of this contribution when the plate location is changed is investigated in this section. Fig. 14 illustrates the simulations performed with the grid Mesh1for the two locations shown in Fig. 12. The diffraction at the trailing edge is obvious for the close-coupled configuration (h/D=0.6) where the jet leaches the plate lower side. On the other hand, no jet/plate hydrodynamic interaction seems to occur when the plate is at h/D=1 and only a low intensity diffracted pressure wave can be observed above the plate in the snapshot in Fig. 14 (b).

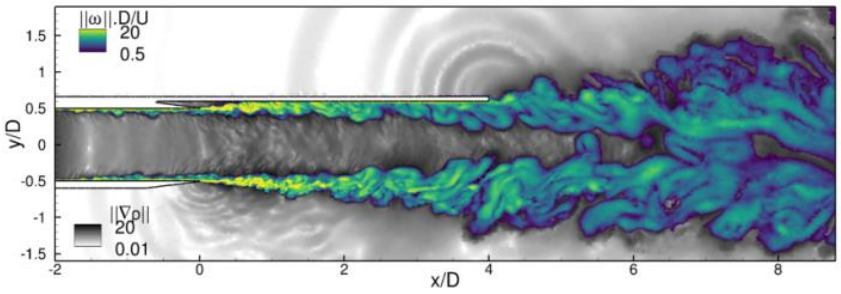

(a) h/D=0.6, L/D=4

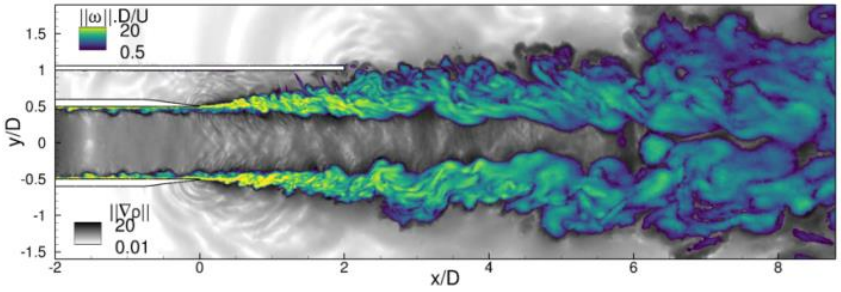

(b) h/D=1, L/D=2

Fig. 14. Snapshots of the simulations. Contours of vorticity magnitude (color) and density gradient (greyscale)

Along the jet centerline, the flow development is not significantly modified by the presence of the plate in both cases as shown in Fig. 15. Conversely, the shear layer development below the plate presented in Fig. 16 illustrates the jet/plate interactions which are quite strong for the lowest plate position.

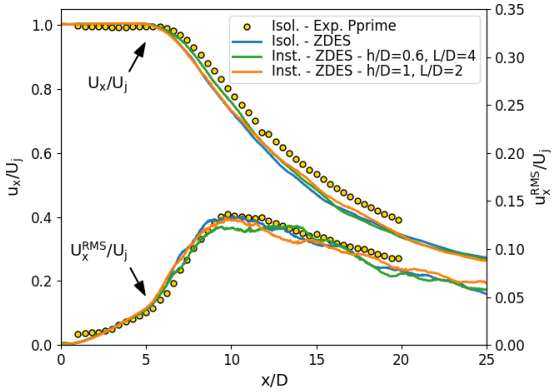

Fig. 15. Profiles along the jet centerline (Isol.: isolated jet, Inst: Installed jet)

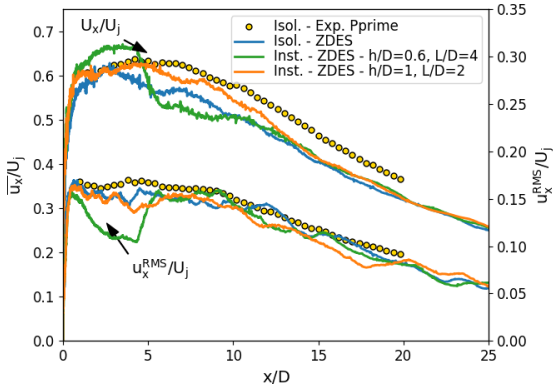

Fig. 16. Profiles along the nozzle lipline below the plate (Isol.: isolated jet, Inst: Installed jet)

Fig. 17 presents near field pressure spectra computed from the probes shown in red in the top picture of Fig. 9. The acoustic shielding by the plate is significant for h/D=0.6, with a reduction of almost 10 dB for all frequencies at x/D=2, r/D=0.98 which is located just above the plate. This shielding cannot be observed with these probes for the h/D=1 case because these probes are located between the jet and the plate in this case. Looking at the probes downstream and above the plate (x/D=4.47, x/D=7.65), the jet/plate interaction noise seems to be limited to 1-2 dB at low frequencies, which may be also an artifact of the insufficient statistical convergence of the results (this topic is addressed in [37]).

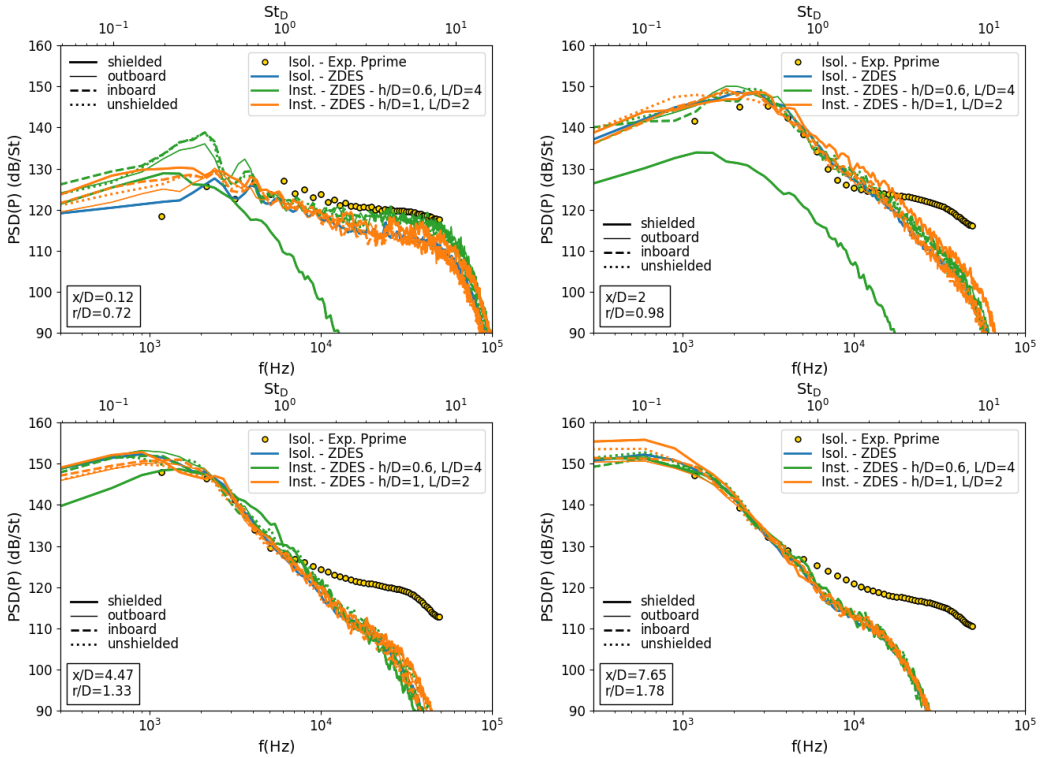

Fig. 17. Pressure spectra in the jet near field

The former observation is strengthened by the integrated noise levels depicted in Fig. 18 and Fig. 19. The comparison with the experimental data confirms the good accuracy of the simulation with the reproduction of the shielding effect of the plate when located at h/D=0.6, whereas modifications are barely visible for the h/D = 1 case most likely because there is no significant interaction between the jet and the plate trailing edge in that case. It is worth mentioning the experimental levels near x/D=0, Φ=180° for the installed configurations are contaminated by structural reflections and shielding of the experimental apparatus and must be disregarded. Additionally, the isolated experimental levels issued from [19] are azimuthally averaged, whereas the simulation is not. The uncertainty of the numerical simulation due to the insufficient statistical convergence of the data globally lies below 1 dB [37]. This value must be kept in mind when comparing simulated and experimental levels for the installed configurations.

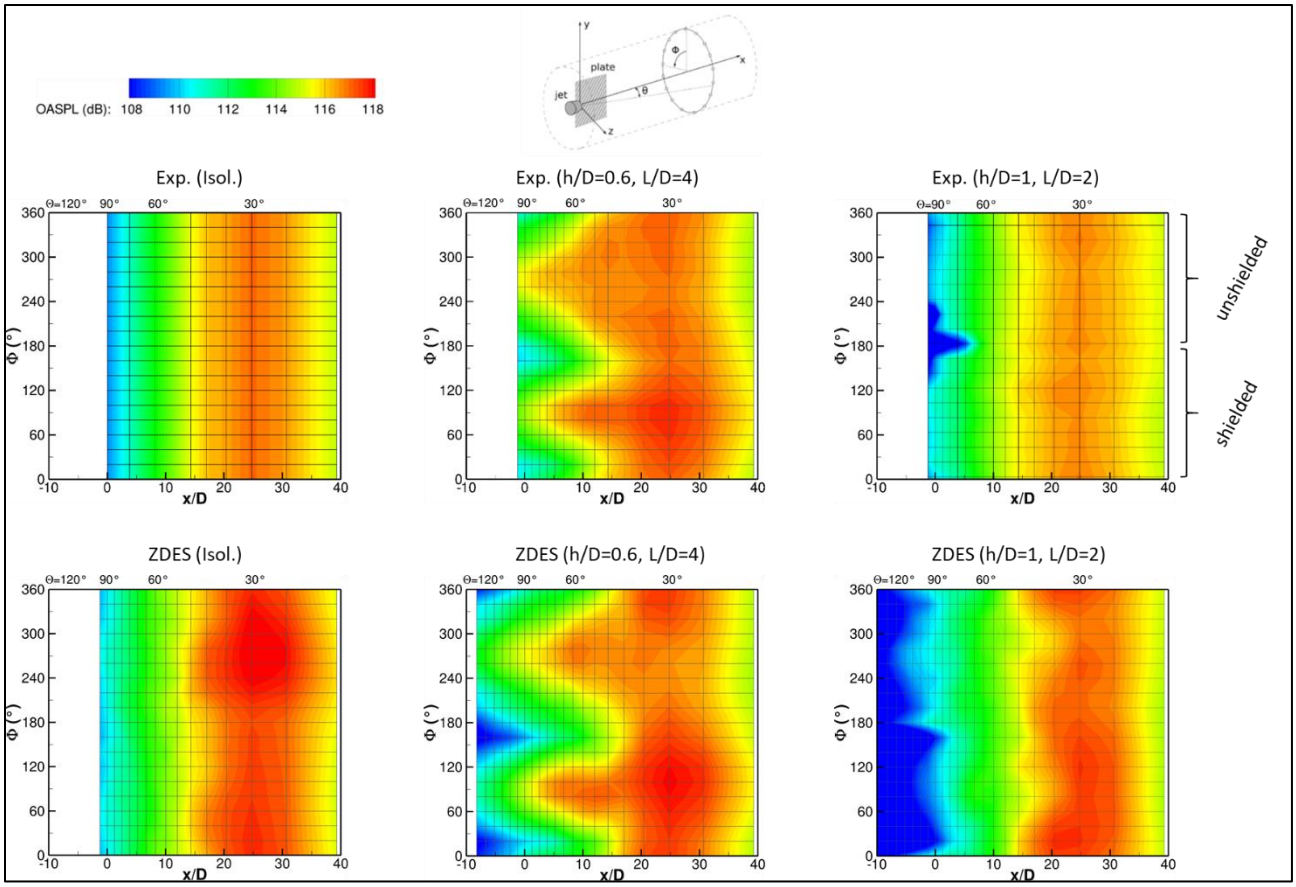

Fig. 18. Cartographies of the integrated farfield noise levels on the azimuthal antenna, case M_j=0.9. St = [0.05 ; 10.00]

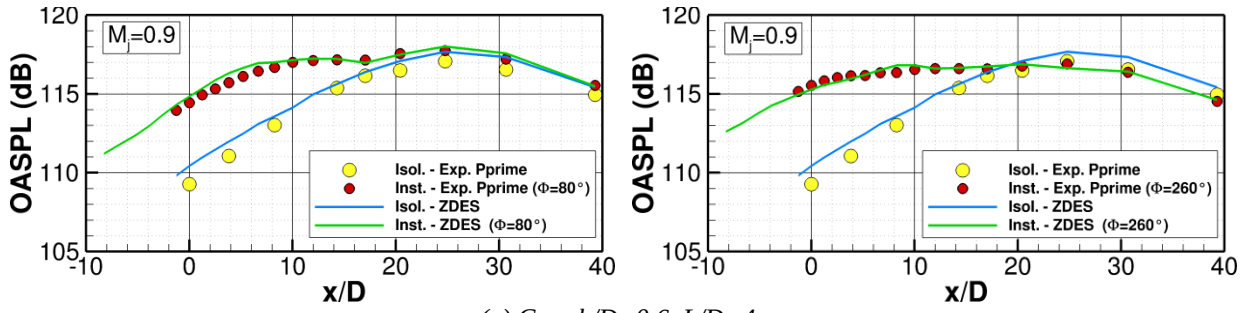

(a) Case h/D=0.6, L/D=4

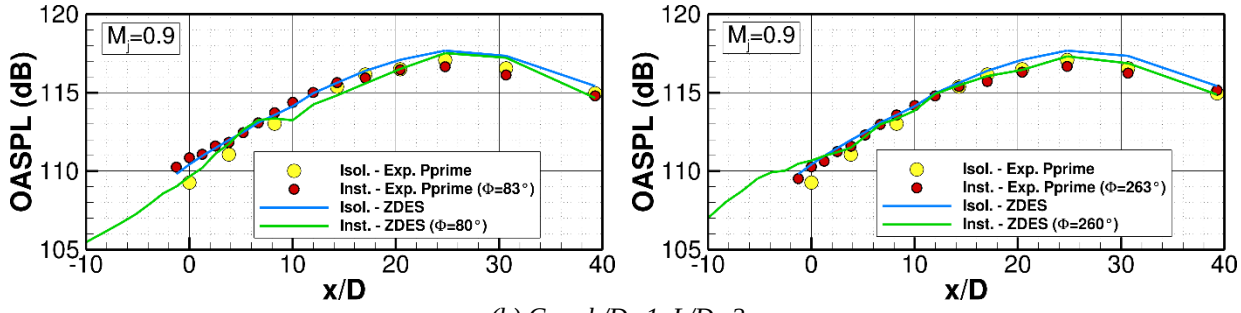

(b) Case h/D=1, L/D=2

Fig. 19. Integrated farfield noise levels on the azimuthal antenna on the shielded (Φ=80°) and unshielded (Φ=260°) sides, case M_j=0.9. St = [0.05 ; 10.00]

As reminded at the beginning of this section, the JSI noise source lies in the diffraction of the wavepackets associated with the jet by the trailing edge of the surface. The acoustic radiation due to the JSI is strong in the direction normal to the plate, as seen for instance in Fig. 14. Due to the linear nature of the JSI noise generation mechanism, the coherence $\gamma^2(f) = |S_{xy}(f)|^2 / S_{xx}(f) S_{yy}(f)$ (where S_{xy} is the cross-spectral density between x and y) between pressure signals extracted along the jet axis –tracking the wavepackets - and at the farfield location θ=90°,ϕ=100° (shielded side) can help educe the JSI amplitude and most energetic frequencies involved in this noise source. As a matter of fact, the coherence maps plotted in Fig. 20 are consistent with the previous comments. Indeed, the higher levels of coherence observed around x/D=4 in the closed-coupled installed jet configuration (h/D=0.6) tend to confirm that the JSI noise is much stronger in this case than in the case h/D=1. Of interest, this result is similar to what was found experimentally in [40], which gives even more confidence in the capability of the present simulations to reproduce the salient features of the JSI noise. Additionally, the JSI noise appears particularly significant in the frequency range St_D=[0.1-1], in agreement with the experimental observations of Cavalieri et al. [45].

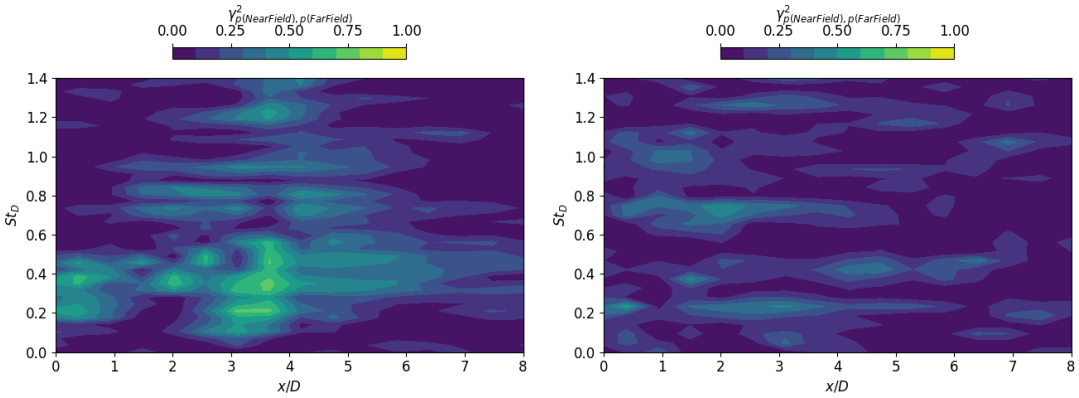

(b) h/D=0.6, L/D=4, M_j=0.9 *(c) h/D=1, L/D=2, M_j=0.9*

Fig. 20. Coherence between sensors located along the jet centerline and a farfield microphone at θ=90°,ϕ=100°

C. Effect of the jet exit Mach number

With jet/surface interaction (JSI) noise reduction in mind, it is attempted to isolate this phenomenon and identify a configuration with little interaction between the jet mean flow and the plate but still a significant installation noise associated with the wavepacket scattering by the plate trailing edge. It was observed in the previous section that the jet self-noise seems to dominate at M_j=0.9 for h/D=1. Jet noise is produced by the flow turbulence and, according to the well-known Lighthill's analogy, the intensity of jet noise scales with the eighth power of the jet exit velocity U_j [46], [47]. More precisely, it scales with $U_j^3 M_0^5$ with $M_0 = U_j/c_0$ the acoustic Mach number and c_0 the sound velocity in the ambient medium. On the other side, JSI noise is produced by the diffraction of the flow turbulence by the trailing edge of the solid surface and its intensity scales with $U_j^3 M_0^2$ [48]. The ratio between jet self noise and JSI noise hence scales with M_0^3 and the contribution of JSI noise is expected to be all the more important as the jet Mach number is low.

Therefore, a simulation at M_j=0.6 is carried out since one can conjecture that the interaction noise will become visible. Note that, in the absence of experimental characterization of the nozzle boundary layer for the M_j=0.6 case, the turbulence generation method used for the M_j=0.9 case was reproduced for M_j=0.6 (see III.B), and the jet exit boundary layer thickness and momentum thickness were only marginally affected (the boundary layer is slightly thicker in the M_j=0.6 case of about 5%). However, it must be noted that in the experiments the jet is maintained isothermal for all Mach numbers thanks to a PID controller [19], but the simulations performed at M_j=0.6 were erroneously run at the same jet total temperature ratio as the M_j=0.9 case which leads to a slightly heated jet in the M_j=0.6 simulations (static temperature ratio T_j/T_∞ = 1.08 in the nozzle exit plane). In turn, the jet exit velocity in the

M_j=0.6 simulations is 4% larger than in the experiments. These discrepancies are not considered significant for flow analyses but may have more influence on the farfield noise predictions since jet noise scales with U_j^8 (see below).

The simulations for the installed jet with h/D=1, L/D=2 at Mach numbers M_j=0.6 and M_j=0.9 are illustrated in Fig. 21. As observed in the previous section, the installation effect on the jet flow aerodynamic development is not significant since the jet vorticity does not impinge the plate.

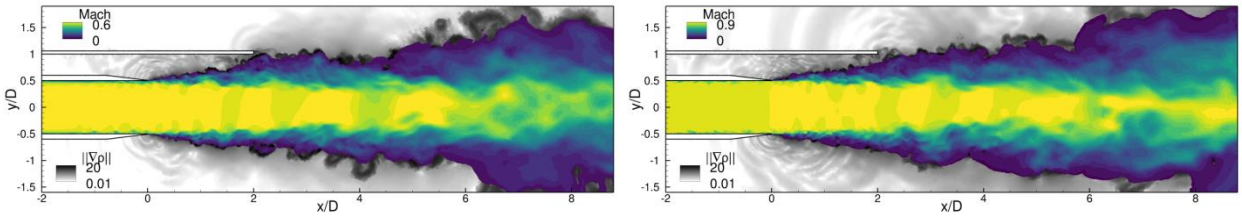

Fig. 21. Snapshots of the simulations of the installed jet at M_j=0.6 (left) and M_j=0.9 (right)

The aerodynamic effect of the jet installation for M_j=0.6 and M_j=0.9 is further assessed with profiles along the jet centerline in Fig. 22 and along the jet lipline (below the plate) in Fig. 23. For both Mach numbers, the results of the installed jet simulation are compared to those of the isolated jet in order to emphasize the installation effect. Along the jet centerline, the installation effect is not significant and the Mach number effect on the isolated jet is reproduced on the installed cases: the lower the Mach number, the shorter the jet. Along the lipline, for each Mach number, one can observe a slight increase of the mean velocity on the installed jet compared to the isolated jet. This may be attributed to a Coandă effect of the plate which induces a small deviation of the jet shear layer, which is not perfectly aligned with the lipline r/D=0.5 and no longer axisymmetric for the installed cases. Apart from this small discrepancy, the aerodynamic effect of the jet installation is not significant both at M_j=0.9 and M_j=0.6.

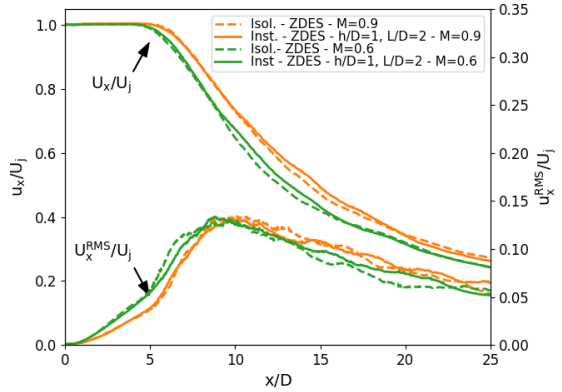

Fig. 22. Profiles along the jet centerline (Isol.: isolated jet, Inst: Installed jet)

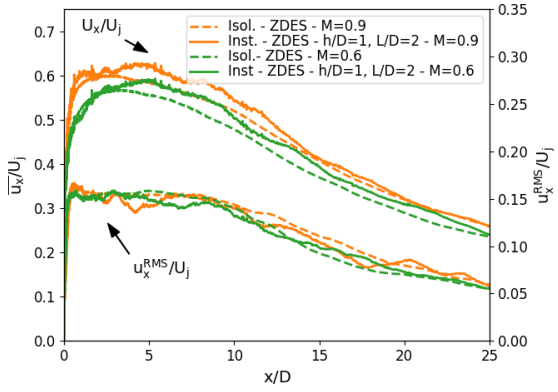

Fig. 23. Profiles along the nozzle lipline below the plate (Isol.: isolated jet, Inst: Installed jet)

The cartographies and profiles of the integrated pressure levels for the M_j=0.6 case are reproduced in Fig. 24 and Fig. 25, respectively. When compared to the results of Fig. 18 and Fig. 19 (b), it is clear that decreasing the jet velocity increases the contribution of JSI on the radiated noise, with a visible azimuthal variation of noise in particular for x/D<10. More quantitatively, simulated levels overestimate the experiments by 2 dB to 3 dB for both the isolated and installed cases. Such an overestimation was not observed for the M_j=0.9 case and it is conjectured that it can be attributed to the error made in the M_j=0.6 simulations jet total temperature ratio, which, as mentioned above, leads to a discrepancy in the jet exit velocity between the simulations and the experiments. Indeed, a preliminary analysis with the semi-empirical jet noise model of Stone *et al.* [49] indicates that this discrepancy could lead to a 1.5 dB overestimation of the OASPL in the M_j=0.6 simulations. A simulation at M_j=0.6 and the correct total temperature ratio is running at the time of writing this paper in order to confirm this estimation.

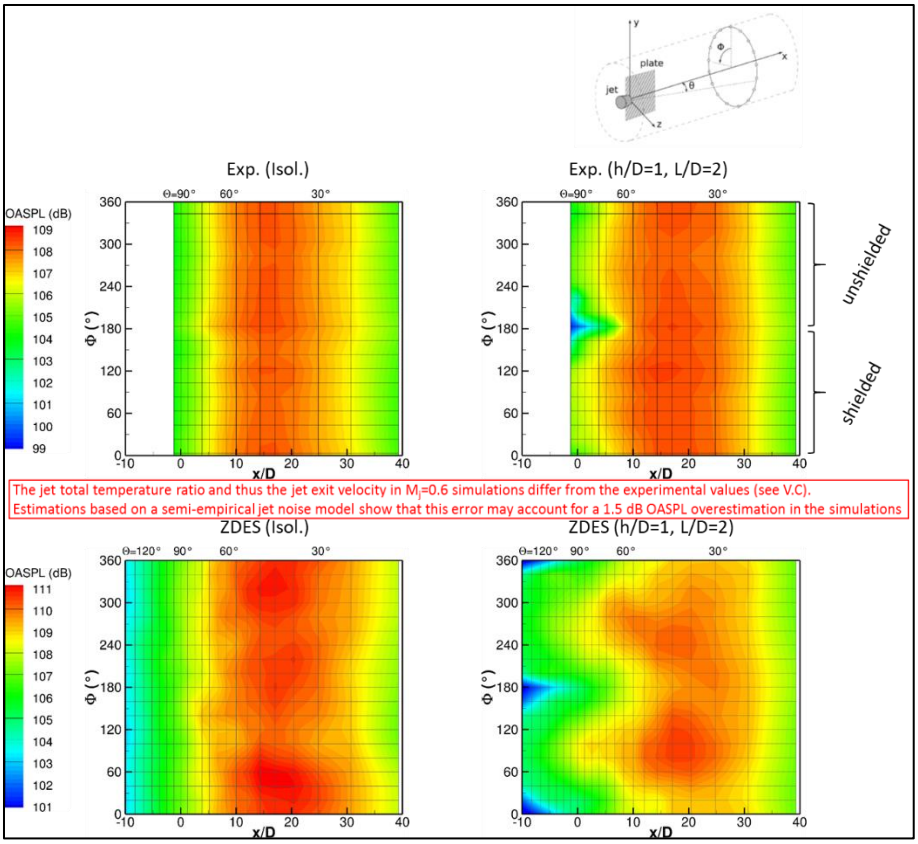

Fig. 24. Cartographies of the integrated farfield noise levels on the azimuthal antenna, case M_j=0.6. St = [0.05 ; 10.00].

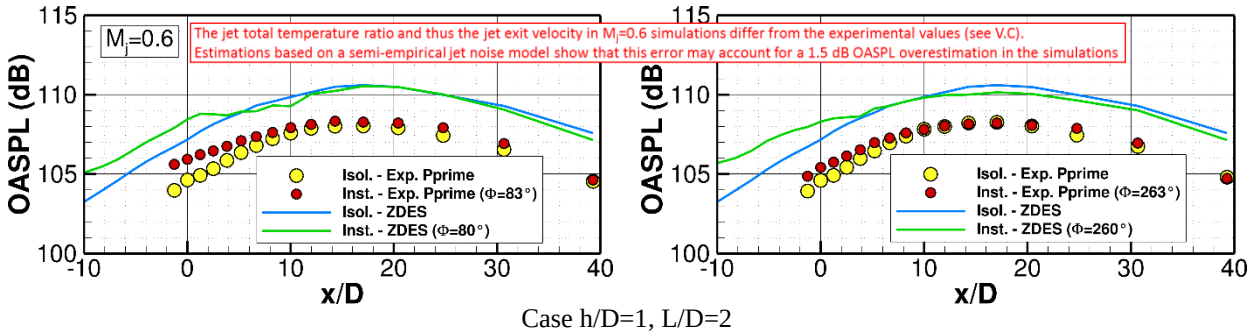

Case h/D=1, L/D=2

Fig. 25. Integrated farfield noise levels on the azimuthal antenna on the shielded (Φ=80°) and unshielded (Φ=260°) sides, case M_j=0.6. St = [0.05 ; 10.00]

In order to investigate further the spatio-temporal organization of the jet near-field pressure fluctuations, the coherence between a reference sensor located at x/D=2, r/D=0 and all other points in the plane (x/D, r/D) is presented in Fig. 26 for the isolated jet at M_j=0.6, in Fig. 27 for the installed jet h/D=1, L/D=2, M_j=0.6 and in Fig. 28 for the installed jet h/D=1, L/D=2, M_j=0.9. In each of these figures, the normalized value of the coherence γ^2 is shown in the left part of the figure and the argument of the cross-spectral density in the right part of the figure. Since it was observed that the relevant frequencies for the JSI noise lie in the range St_D=[0.1, 1], these quantities are plotted for St_D=0.1, 0.5 and 1.

The analysis of the results for the isolated jet (Fig. 26) is consistent with the well-known wavepacket structure of the pressure fluctuations associated with the jet. These are dominant for mid-frequencies St_D=0.5 and the phase plots help educe the wavepackets phase speed and streamwise correlation length. This is not observed at low frequencies

St_D=0.1 and appears evanescent at St_D=1, in agreement with experimental observations [45]. The comparison of Fig. 26 and Fig. 27 emphasizes the JSI noise generation mechanism. At St_D=0.5, where the jet wavepacket is dominant, the coherence amplitude values remain large above the plate and the phase plot shows the scattering of the wavepacket by the plate trailing edge. Finally, the Mach number effect for the installed jets can be assessed by comparing Fig. 27 (M_j=0.6) and Fig. 28 (M_j=0.9). The coherence values at St_D=0.5 above the plate are lower at M_j=0.9 than at M_j=0.6, which tends to show that the noise source due to the scattering of the wavepacket is not dominant compared to the "direct" contribution of the wavepacket itself at high Mach numbers. This is supported by the coherence spectra maps depicted in Fig. 29 and explains the results obtained for the farfield noise levels shown previously. Moreover, it is consistent with experimental findings [44] and with the discussion at the beginning of this section about the Mach number scaling of jet noise and JSI noise.

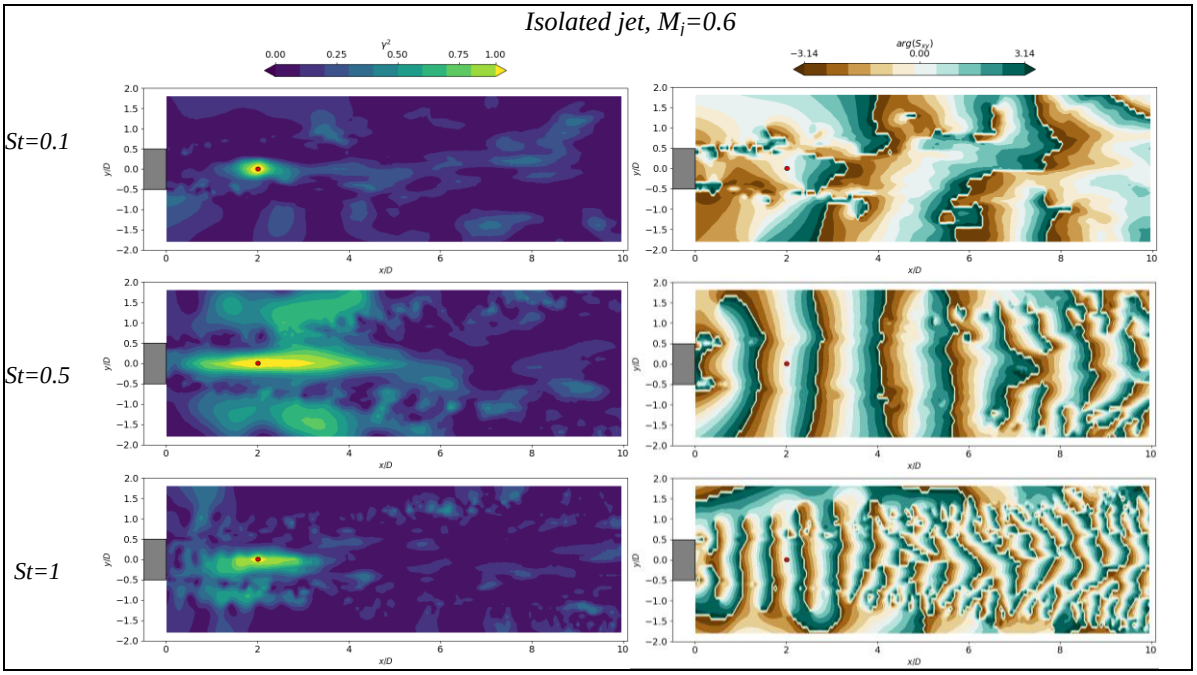

Fig. 26. Isolated jet, M_j=0.6. Maps of coherence (left) and cross-spectral density phase (right). The reference point used for the computation is located at x/D=2, r/D=0, emphasized in red in the plots

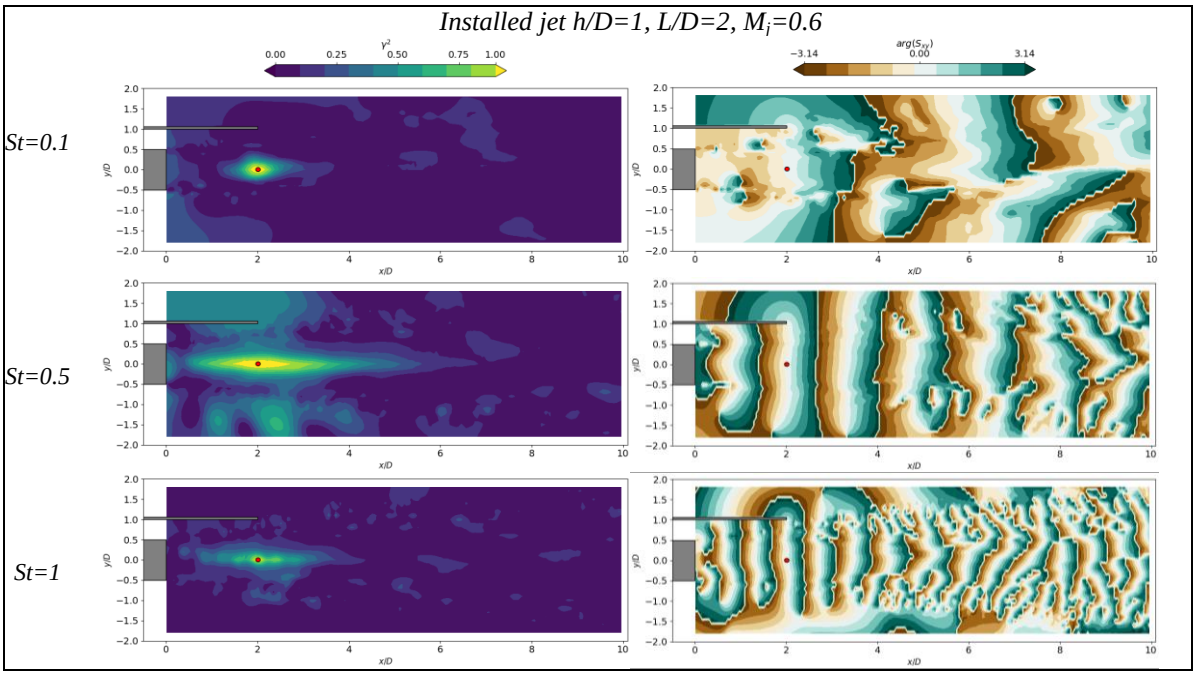

Fig. 27. Installed jet h/D=1, L/D=2, M_j=0.6. Maps of coherence (left) and cross-spectral density phase (right). The reference point used for the computation is located at x/D=2, r/D=0, emphasized in red in the plots

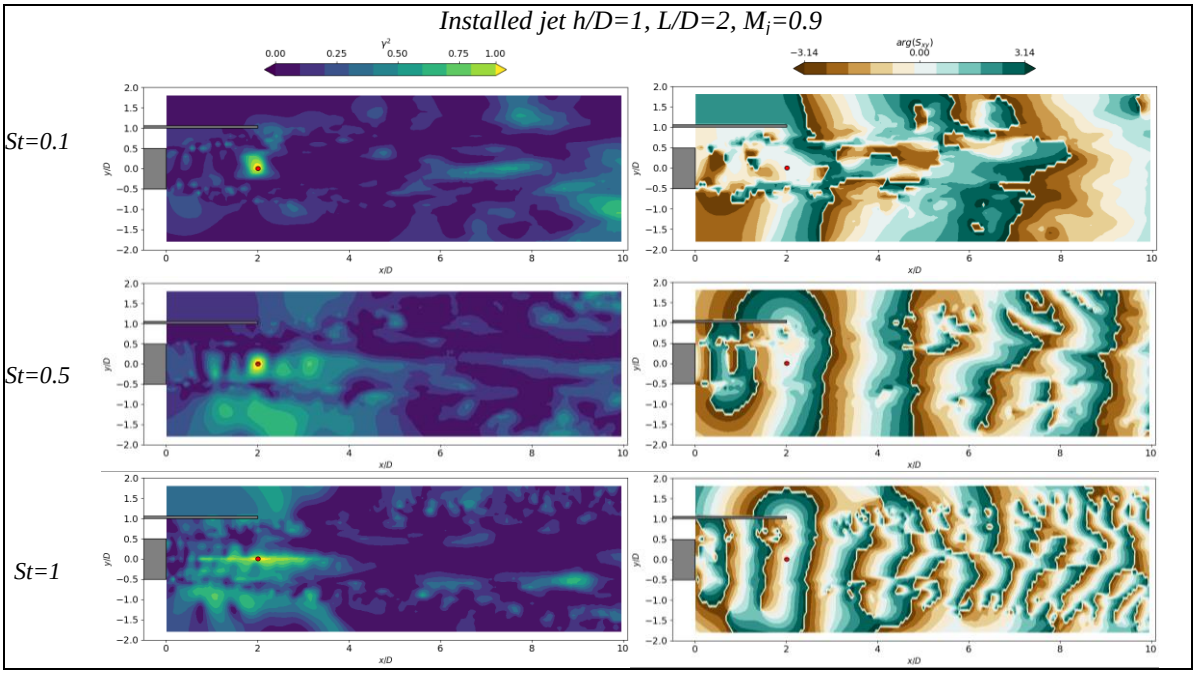

Fig. 28. Installed jet h/D=1, L/D=2, M_j=0.9. Maps of coherence (left) and cross-spectral density phase (right). The reference point used for the computation is located at x/D=2, r/D=0, emphasized in red in the plots

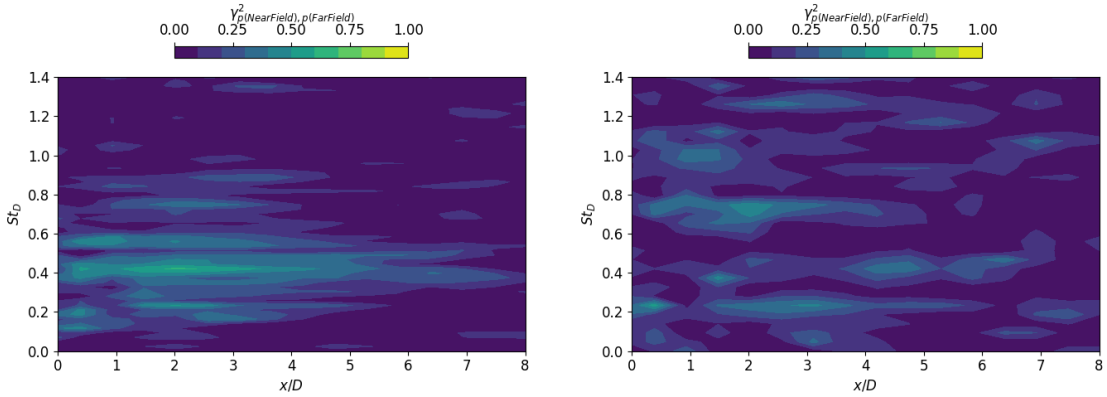

(a) h/D=1, L/D=2, M_j=0.6 *(b) h/D=1, L/D=2, M_j=0.9*

Fig. 29. Coherence spectra maps between sensors located along the jet centerline and a farfield microphone at θ=90°,φ=100°

VI. Towards the application to an industry-relevant test case

The final section of this paper is devoted to the application of the numerical methodology based on ZDES and unstructured meshes to a configuration of interest for industrial applications. A business-jet-like case composed of a dual mixed flow nozzle, a fuselage and a horizontal tail plane (HTP) was chosen as shown in Fig. 30. In this case, the jet/surface interaction noise is not really a concern since the jet/surface distance is very large, however the HTP encounters strong pressure fluctuations coming from the jet which can cause structural damage. This phenomenon is known as acoustic fatigue. This configuration is challenging for simulation methods because acoustic pressure waves need to be transported from the jet up to the HTP, in other words a large distance needs to be meshed with small cells. In the present case, the mesh used was inspired by the topologies presented in sections IV and V as illustrated in Fig. 30. Of interest, the cell sizes corresponding to Mesh2 of the isolated single stream jet were targeted (in terms of cell size distributions along the jet centerline, lipline and in the acoustic propagation area), resulting in 300.10^6 mesh cells. The surfaces enclosing the noise sources used to extract the CFD data to feed the FWH solver are shown in Fig. 31.

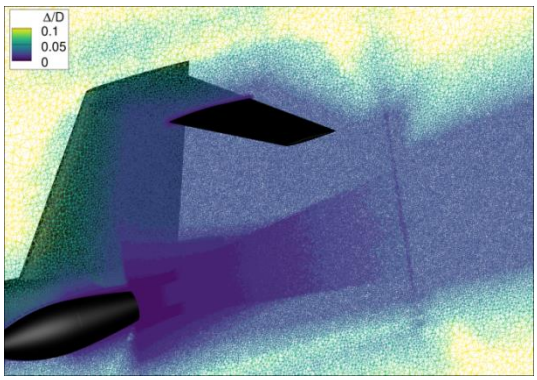

Fig. 30. Illustration of the mesh used for the business-jet case

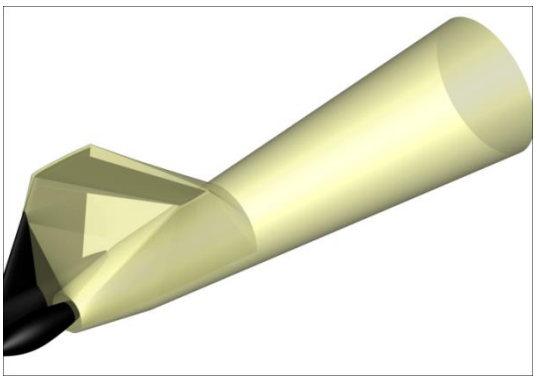

Fig. 31. Extraction surfaces for the FWH acoustic analysis

The setup of the simulation followed the steps defined for the study of the previous configurations. First, a ZDES simulation of the isolated nozzle was performed to focus on the positioning and sizing of the tripping cylinders. The nozzle exit boundary layer thickness was estimated from preliminary wind tunnel tests measurements and the tripping cylinders were placed in order to reach such thickness with plausible resolved turbulence. This setup was then introduced in the mesh of the complete configuration depicted in Fig. 30. As illustrated in Fig. 32, the ZDES simulation is running at the time of writing this paper. One can see in Fig. 32 that the acoustic waves are indeed propagated towards the horizontal tail plane.

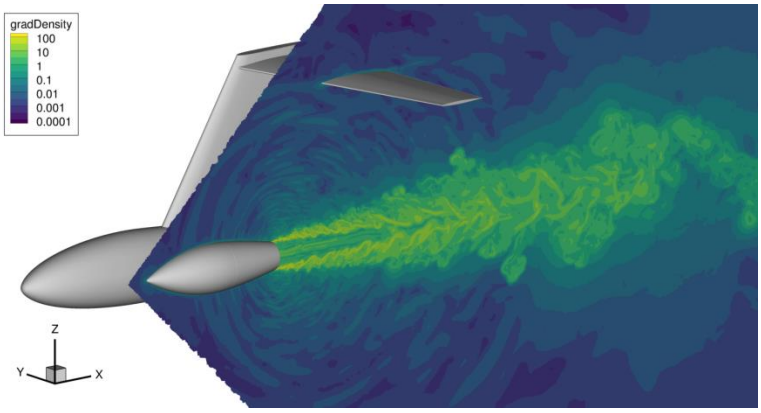

Fig. 32. Illustration of the ZDES simulation (transient stage, work in progress)

VII. Conclusions, challenges and perspectives

In this paper, the use of ZDES with unstructured grids is assessed for the prediction of jet noise. The approach is tested on reference cases of increasing complexity, namely an isolated jet, an installed jet and an industrial configuration.

The study of the isolated jet includes a grid sensitivity analysis which gives confidence in the robustness of the method. The results are in very good agreement with experimental data and state-of-the-art simulations for all metrics (flow and noise) and provide a significant improvement with respect to previous simulations with structured grids of comparable size. This approach was therefore used to investigate jet/surface interaction noise on a simplified configuration. The accuracy of the simulation was verified through a comparison with the available experimental data. The influence of the plate location and the jet exit Mach number were scrutinized, and the salient spatio-temporal features of the jet/surface interaction (JSI) noise were found to be well accounted for by the simulations. In line with the existing experimental and numerical literature, moving the plate away from the jet decreases the intensity of the JSI noise, and increasing the jet exit Mach number weakens the scattering of the wavepacket by the plate trailing edge. Finally, an industrial configuration was considered to demonstrate the applicability of the method to complex cases. This work is still in progress and final results will be reported in future publications.

Throughout the three studies presented in this paper, a number of challenges were outlined. In terms of numerics, low dissipation schemes for unstructured grids with general cell shapes are needed. Indeed, a standard upwind scheme was used in the present work, which is known to be inappropriate for aeroacoustics simulations. The use of very fine meshes with mostly isotropic cells in areas of interest certainly helped to achieve satisfying results, but hybrid central/upwind schemes adapted for unstructured meshes (e.g. [50] [51] [9] [52]) would be beneficial.

Large simulation times are mandatory for complex cases (azimuthal averaging compensates for small time samples in axisymmetric cases), and more generally to generate CFD datasets of duration comparable to the experimental ones. This entails the need for new generation CFD solvers with enhanced HPC capabilities. Some issues at stakes in this domain are scalability, vectorization, cache memory management to avoid memory-bound codes, management of heterogeneous HPC architectures including GPUs, etc. These points are all the more complicated as they are also impacted by the numerical schemes used. It is noteworthy that such HPC developments for large simulation cases are also mandatory for FWH codes.

Another key issue is the data management. Indeed, parallel I/O and in-memory co-processing have to be implemented in order to extract as much data as possible from these large simulations. In particular, on-the-fly co-processing for the FWH radiation is appealing because it would avoid the storage of large datasets, but on the other hand it would prevent a posteriori investigations on the sensibility of the farfield results to the FWH code settings, including the location of the farfield numerical microphones.

As mentioned previously, one objective of the present work was to move from legacy structured grids to unstructured meshes to deal with complex geometries. Such an approach was used with success, however it must be stressed that scale resolving simulations require a special attention and control of mesh sizes, which still makes the mesh generation an iterative and not completely automated task. The use of adaptive mesh refinement is interesting but its application to unsteady scale resolving simulations also raises fundamental questions which need to be addressed.

Beyond these numerical and computer-science issues, jet noise physics and modelling still remain an active field of research for which on-going efforts include, among many other topics, closed-loop active noise reduction techniques informed by the nature of JSI noise, fast and reliable modelling and improvement of noise radiation formulations to account for multiple acoustic reflecting surfaces.

Acknowledgments

This work has been performed in the frame of the EU DJINN (Decrease Jet Installation Noise) project. DJINN project receives funding from the European Union's Horizon 2020 research and innovation programme under grant agreement No 861438. DJINN is a collaborative effort between CFD-Berlin (coordinator), Airbus SAS, Dassault Aviation, Safran Aircraft Engines, Rolls-Royce Deutschland, ONERA, DLR, University of Southampton, CERFACS, Imperial College London, von Karman Institute, CNRS, and Queen Mary University of London.

The authors are grateful to Dr Peter Jordan (Pprime), Dr Matteo Mancinelli (Pprime, now at Uni Roma Tre), Dr Eduardo Martini (Pprime) and Dr Filipe Ramos do Amaral (Pprime) for sharing experimental data and for fruitful discussions on JSI noise and control.

Part of this work was granted access to the HPC resources of CINES under the allocation 2021-A0102A12442 made by GENCI.

References

[1] E. Commission, "Flightpath 2050, Europe's Vision for Aviation," Tech. Rep. European Commission, 2011. doi: 10.2777/50266.

[2] D. J. Bodony and S. K. Lele, "Current Status of Jet Noise Predictions Using Large-Eddy Simulation," *AIAA Journal*, vol. 46 (2), pp. 364-380, 2008. doi: 10.2514/1.24475.

[3] S. K. Lele and J. W. Nichols, "A second golden age of aeroacoustics?," *Philosophical Transactions of the Royal Society A*, vol. 372, p. 20130321, 2014. doi: 10.1098/rsta.2013.0321.

[4] A. S. Lyrintzis and M. Coderoni, "The Use of LES in Jet Aeroacoustics," in *AIAA SciTech Forum, 7-11 January 2019, San Diego, California. AIAA Paper 2019-0633*, 2019. doi: 10.2514/6.2019-0633.

[5] "European Project H2020: Decrease Jet InstallatioN Noise (DJINN)," [Online]. Available: https://djinn.online/.

[6] F. Gand, M. Huet, T. Le Garrec and F. Cléro, "Jet noise of a UHBR nozzle using ZDES: external boundary layer thickness and installation effects," in *23rd AIAA/CEAS Aeroacoustics Conference, AIAA Paper 2017-3526*, 2017.

[7] F. Sartor, F. Gand, M. Huet, S. Beneddine and D. Sipp, "Numerical Study of a Double-Stream Jet: ZDES Simulation, Stability Analysis and Noise Reduction," in *34th AIAA Applied Aerodynamics Conference, AIAA Paper 2016-3259*, 2016.

[8] J. Tyacke, Z. Wang and P. Tucker, "LES-RANS of Installed Ultra-High-Bypass-Ratio Coaxial Jet Aeroacoustics with Flight Stream," *AIAA Journal*, pp. 1-22, 2019. doi: 10.2514/1.j057057.

[9] H. Xia, P. G. Tucker, S. Eastwood and M. Mahak, "The influence of geometry on jet plume development," *Progress in Aerospace Sciences*, vol. 52, p. 56–66, 2012. doi: 10.1016/j.paerosci.2011.12.003.

[10] A. Uzun and M. Y. Hussaini, "Some Issues in Large-Eddy Simulations for Chevron Nozzle Jet Flows," *Journal of Propulsion and Power*, vol. 28 (2), pp. 246-258, 2012. doi: 10.2514/1.B34274.

[11] M. Huet, "Influence of boundary layers resolution on heated, subsonic, high Reynolds number jet flow and

noise," in *19th AIAA/CEAS Aeroacoustics Conference, may 27--29 2013, Berlin, Germany. AIAA Paper 2013-2141*, 2013.

[12] M. Lorteau, F. Clero and F. Vuillot, "Analysis of noise radiation mechanisms in hot subsonic jet from a validated large eddy simulation solution," *Physics of Fluids,* vol. 27, p. 075108, 2015. doi: 10.1063/1.4926792.

[13] G. Pont, P. Brenner, P. Cinnella, B. Maugars and J.-C. Robinet, "Multiple-correction hybrid k-exact schemes for high-order compressible RANS-LES simulations on fully unstructured grids," *Journal of Computational Physics,* vol. 350, p. 45–83, 2017. doi: 10.1016/j.jcp.2017.08.036.

[14] G. A. Brès, F. E. Ham, J. W. Nichols and S. K. Lele, "Unstructured Large-Eddy Simulations of Supersonic Jets," *AIAA Journal,* p. 1–21, 1 2017. doi: 10.2514/1.J055084.

[15] A. Fosso-Pouangué, M. Sanjosé, S. Moreau, G. Daviller and H. Deniau, "Subsonic Jet Noise Simulations Using Both Structured and Unstructured Grids," *AIAA Journal,* vol. 53 (1), pp. 55-69, 2015. doi: 10.2514/1.J052380.

[16] M. Sanjose, A. Fosso-Pouangué, S. Moreau, G. Wang and T. Padois, "Unstructured LES of the baseline EXEJET dual-stream jet," in *20th AIAA/CEAS Aeroacoustics Conference, 16-20 June 2014, Atlanta, GA. AIAA 2014-3037*, 2014. doi: 10.2514/6.2014-3037.

[17] A. P. Markesteijn, V. Gryazev, S. A. Karabasov, R. S. Ayupov, L. A. Benderskiy and D. A. Lyubimov, "Flow and Noise Predictions of Coaxial Jets," *AIAA Journal,* p. 1–14, 10 2020. doi: 10.2514/1.j058881.

[18] M. Zhu, C. Pérez Arroyo, A. Fosso-Pouangué, M. Sanjose and S. Moreau, "Isothermal and heated subsonic jet noise using large eddy simulations on unstructured grids," *Computers and Fluids,* vol. 171, pp. 166-192, 2018.

[19] G. A. Brès, P. Jordan, V. Jaunet, M. Le Rallic, A. V. G. Cavalieri, A. Towne, S. K. Lele, T. Colonius and O. T. Schmidt, "Importance of the nozzle-exit boundary-layer state in subsonic turbulent jets," *Journal of Fluid Mechanics,* vol. 851, pp. 83-124, 2018. doi: 10.1017/jfm.2018.476.

[20] L. Cambier, S. Heib and S. Plot, "The Onera elsA CFD software: input from research and feedback from industry," *Mechanics and Industry,* vol. 14, pp. 159-174, 2013. doi: 10.1051/meca/2013056.

[21] I. Mary and P. Sagaut, "Large Eddy Simulation of Flow around an Airfoil Near Stall," *AIAA Journal,* vol. 40, pp. 1139-1145, 2002.

[22] S. Deck, "Recent Improvements of the Zonal Detached Eddy Simulation (ZDES) Formulation," *Theoretical and Computational Fluid Dynamics,* vol. 26, pp. 523-550, 2012. doi: 10.1007/s00162-011-0240-z.

[23] S. Deck, F. Gand, V. Brunet and S. Ben Khelil, "High-fidelity simulations of unsteady civil aircraft aerodynamics: stakes and perspectives. Application of zonal detached eddy simulation," *Philosophical Transactions of the Royal Society A,* 2014. doi: 10.1098/rsta.2013.0325.

[24] F. Gand and M. Huet, "On the generation of turbulent inflow for hybrid RANS/LES jet flow simulations," *Computers & Fluids,* vol. 216, p. 104816, 2 2021. doi: 10.1016/j.compfluid.2020.104816.

[25] C. Bogey and O. Marsden, "Simulations of Initially Highly Disturbed Jets with Experiment-Like Exit Boundary Layers," *AIAA Journal,* p. 1–14, 2 2016. doi: 10.2514/1.J054426.

[26] S. Deck and R. Laraufie, "Numerical investigation of the flow dynamics past a three-element aerofoil," *Journal of Fluid Mechanics,* vol. 732, pp. 401-444, 2013. doi: 10.1017/jfm.2013.363.

[27] P. Spalart, W. Jou, M. Strelets and S. Allmaras, "Comments on the feasibility of LES for wings, and on a hybrid RANS/LES approach," in *First AFOSR International Conference on DNS/LES.*, 1997.

[28] P. R. Spalart and S. R. Allmaras, "A One-Equation Turbulence Model for Aerodynamic Flows," *La Recherche Aérospatiale,* vol. 1, pp. 5-21, 1994.

[29] S. Deck and N. Renard, "Towards an enhanced protection of attached boundary layers in hybrid RANS/LES methods," *Journal of Computational Physics,* vol. 400, 2020. doi: 10.1016/j.jcp.2019.108970.

[30] S. Deck, N. Renard, R. Laraufie and P. Sagaut, "Zonal Detached Eddy Simulation (ZDES) of a spatially developing flat plate turbulent boundary layer over the Reynolds number range 3 150 < Reθ < 14 000," *Physics of Fluids,* vol. 26, p. 025116, 2014. doi: 10.1063/1.4866180.

[31] S. Deck, P.-E. Weiss and N. Renard, "A rapid and low noise switch from RANS to WMLES on curvilinear grids with compressible flow solvers," *Journal of Computational Physics,* vol. 363, pp. 231-255, 2018. doi: 10.1016/j.jcp.2018.02.028.

[32] J. E. Ffowcs Williams and D. L. Hawkings, "Sound generation by turbulence and surfaces in arbitrary motion," *Philosophical Transactions for the Royal Society of London,* vol. A264, pp. 321-342, 1969.

[33] G. Rahier, M. Huet and J. Prieur, "Additional terms for the use of Ffowcs Williams and Hawkings surface integrals in turbulent flows," *Computers & Fluids,* vol. 120, pp. 158-172, 2015. doi: 10.1016/j.compfluid.2015.07.014.

[34] M. L. Shur, P. R. Spalart and M. K. Strelets, "Noise prediction for increasingly complex jets. Part II: Applications," *International Journal of Aeroacoustics,* vol. 4, pp. 247-266, 2005. doi: 10.1260/1475472054771385.

[35] S. Mendez, M. Shoeybi, S. K. Lele and P. Moin, "On the Use of the Ffowcs Williams-Hawkings Equation to Predict Far-Field Jet Noise from Large-Eddy Simulations," *International Journal of Aeroacoustics,* vol. 12, pp. 1-20, 2013. doi: 10.1260/1475-472x.12.1-2.1.

[36] G. Rahier, "Approximate computation of reflection and shadow effects of a body in an acoustic field by Kirchhoff method," *in preparation.*

[37] M. Huet, F. Gand and G. Rahier, "Simulation of jet installation effects at Mach=0.9: influence of numerical methodology and physical insights," *Flow, Turbulence and Combustion,* submitted for publication.

[38] A. Cavalieri, P. Jordan, W. Wolf and Y. Gervais, "Scattering of wave packets by a flat plate in the vicinity of a turbulent jet," *Journal of Sound and Vibration,* vol. 333, p. 6516–6531, 2014. doi: 10.1016/j.jsv.2014.07.029.

[39] P. A. S. Nogueira, J. R. L. N. Sirotto, R. F. Miotto, A. V. G. Cavalieri, J. A. Cordioli and W. R. Wolf, "Acoustic radiation of subsonic jets in the vicinity of an inclined flat plate," *The Journal of the Acoustical Society of America,* vol. 146, p. 50–59, July 2019. doi: 10.1121/1.5115006.

[40] S. Piantanida, V. Jaunet, J. Huber, W. R. Wolf, P. Jordan and A. V. G. Cavalieri, "Scattering of turbulent-jet wavepackets by a swept trailing edge," *The Journal of the Acoustical Society of America,* vol. 140, p. 4350–4359, 8 2016. doi: 10.1121/1.4971425.

[41] G. Faranosov, O. P. Bychkov, V. Kopiev, L. F. Soares and A. V. Cavalieri, "The Modeling of Jet-Plate Interaction Noise in the Presence of Co-Flow," in *25th AIAA/CEAS Aeroacoustics Conference*, 2019. doi: 10.2514/6.2019-2492.

[42] O. Bychkov, G. Faranosov, V. Kopiev, V. Kopiev, I. Moralev and P. Kazansky, "Plasma-based active closed-loop control of instability waves in unexcited turbulent jet. Part 2. Installed jet.," in *25th AIAA/CEAS Aeroacoustics Conference, 2019. AIAA Paper 2019-2558*, 2019.

[43] V. Kopiev, G. Faranosov, O. Bychkov, V. Kopiev, I. Moralev and P. Kazansky, "Active control of jet-plate interaction noise for excited jets by plasma actuators," *Journal of Sound and Vibration,* vol. 484, p. 115515, 2020. doi: https://doi.org/10.1016/j.jsv.2020.115515.

[44] M. Mancinelli, P. Jordan, A. Lebedev and R. Kari, "Real-time jet-plate interaction noise estimation based on near-field sensor readings," in *28th AIAA/CEAS Aeroacoustics 2022 Conference*, 2022. doi: 10.2514/6.2022-2871.

[45] A. V. G. Cavalieri, D. Rodríguez, P. Jordan, T. Colonius and Y. Gervais, "Wavepackets in the velocity field of turbulent jets," *Journal of Fluid Mechanics,* vol. 730, pp. 559-592, 2013.

[46] M. J. Lighthill, "On sound generated aerodynamically I. General theory," *Proceedings of the Royal Society A,* vol. 211, pp. 564-587, 1952.

[47] M. J. Lighthill, "On sound generated aerodynamically II. Turbulence as a source of sound," *Proceedings of the Royal Society A,* vol. 222, pp. 1-32, 1954.

[48] J. E. Ffowcs Williams and L. H. Hall, "Aerodynamic sound generation by turbulent flow in the vicinity of a scattering half plane," *Journal of Fluid Mechanics,* vol. 40, pp. 657-670, 1970.

[49] J. R. Stone, D. E. Groesbeck and C. L. Zola, "Conventional profile coaxial jet noise prediction," *AIAA Journal,* vol. 21, p. 336–342, 3 1983. doi: 10.2514/3.8077.

[50] G. Pont, "Self adaptive turbulence models for unsteady compressible flows," 2015.

[51] M. L. Shur, P. R. Spalart and M. K. Strelets, "Noise prediction for increasingly complex jets. Part I: Methods and tests," *International Journal of Aeroacoustics,* vol. 4, p. 213–246, 2005. doi: 10.1260/1475472054771376.

[52] Z. N. Wang, A. Proenca, J. Lawrence, P. G. Tucker and R. Self, "Large-Eddy-Simulation Prediction of an Installed Jet Flow and Noise with Experimental Validation," *AIAA Journal,* p. 1–10, 3 2020. doi: 10.2514/1.j058921.